PHYSICAL REVIEW B **89**, 060102(R) (2014)

Local fivefold symmetry in liquid and undercooled Ni probed by x-ray absorption spectroscopy and computer simulations

A. Di Cicco,[1] F. Iesari,[1] S. De Panfilis,[2] M. Celino,[3] S. Giusepponi,[3] and A. Filipponi[4]

[1]*Physics Division, School of Science and Technology, Università di Camerino, I-62032 Camerino (MC), Italy*

[2]*Istituto Italiano di Tecnologia, Centre for Life Nanoscience–IIT@Sapienza,Viale Regina Elena 291, I-00161, Roma, Italy*

[3]*ENEA, Italian National Agency for New Technologies, Energy and Sustainable Economic Development, C.R. Casaccia, Via Anguillarese 301, I-00123 Roma, Italy*

[4]*Dipartimento di Scienze Fisiche e Chimiche, Università degli Studi dell'Aquila, I-67100 L'Aquila, Italy*

(Received 6 November 2013; revised manuscript received 17 January 2014; published 12 February 2014)

Presence and significance of fivefold configurations in liquid metals are investigated by combining x-ray absorption spectroscopy and computer simulations (molecular dynamics and reverse Monte Carlo) in liquid and undercooled liquid nickel. We show that icosahedral short-range ordering (ISRO), probed by common-neighbor (CNA) and spherical invariant ($\hat{W}_6$) analysis, involves a limited fraction (14–18% in undercooled nickel for different structural models) of local atomic configurations. The emerging picture for the liquid structure is that of a mixture of nearly icosahedral structures embedded in a disordered network mainly composed of fragments of highly distorted icosahedra (40–45% of the total), structures reminiscent of the crystalline phase, and other configurations.

DOI: 10.1103/PhysRevB.89.060102 PACS number(s): 61.25.Mv, 61.20.Ja

The nature of local point symmetry in simple monoatomic liquids has been a fundamental open question for almost 40 years of computational and experimental studies, following Frank's initial hypothesis [1] about the presence of icosahedral short-range ordering (ISRO) in liquids. The presence of such close-packed fivefold configurations, incompatible with translational symmetry but favored by energetic considerations, was considered as a possible explanation for the peculiar undercooling properties of liquid metals studied by Turnbull in the early fifties [2]. Crystal nucleation [3] is hampered by the positive liquid-crystal interfacial energy, resulting in the possibility of bringing a liquid sample into a metastable (undercooled) molten state below the melting temperature T_m. Experiments based on repeated temperature cycles on droplet specimens are commonly used to infer nucleation rate [4] and information on nucleation barriers [5]. The debate about the presence and amount of ISRO in undercooled liquids is still open, in part because of the experimental difficulties in accessing deeply undercooled states and the limited structural information supplied by x-ray diffraction experiments.

In recent decades, several computational and experimental studies were devoted to investigating locally preferred structures in simple atomic liquids (see, for example, Refs. [6–10]), and most of these works support the existence and importance of ISRO. X-ray absorption spectroscopy (XAS), which is suitable to investigate liquid matter [11] and sensitive to higher order distribution functions and local geometry, was previously exploited for undercooled Pd [12] and Cu [13]. For undercooled copper, it was shown that the fraction of nearly icosahedral configurations is around 10%, evidence later supported by molecular dynamics (MD) simulations [14,15]. In the case of liquid and undercooled nickel, an element very close to copper in its structural properties, MD simulations [16,17] and diffraction experiments [18,19] indicated that a large fraction of atoms show local icosahedral symmetry. However, the detailed structural analysis reported in Ref. [19], shows that the fraction of nearly icosahedral configurations is similar to that found in liquid Cu [13].

Stimulated by these recent results, we have performed an extensive investigation on liquid and undercooled nickel, combining state-of-the-art experimental and computational techniques, for the purpose of evaluating the amount of ISRO and establishing reliable criteria for assessing the nature of local geometries in close-packed liquids. In this work, the local order probed by XAS is analyzed using a reverse Monte Carlo (RMC) [20,21] approach, yielding structure models compatible with the measurements. Realistic models for the liquid structures are also obtained using advanced MD simulations. Reliable information about the presence and amount of ISRO in MD and RMC models is extracted using a suitable geometrical analysis.

The XAS experiment was performed at the BM29 beamline [22] of the European Synchrotron Radiation Facility (ESRF, Grenoble). Samples for high-temperature measurements were prepared from submicrometric Ni and alumina (Al_2O_3) powder mixtures with a 1:20 mass ratio that were suspended in alcohol, filtered, and pressed into 100-μm-thick, 13-mm-diameter pellets. The furnace consisted of a 130-mm-diameter cylindrical Pyrex glass vessel with a suitable window for simultaneous x-ray diffraction (XRD) and XAS data collection. The pellets were placed inside the crucible of the furnace and the heat treatments were performed under high-vacuum conditions of $P \simeq 10^{-5}$ mbar. Similar to the Pd case [12], alumina was not found to react with nickel at the temperatures involved in the experiment. Temperature measurements were performed using a high-temperature pyrometer (estimated uncertainty is 20 K). The temperature behavior of the sample and its phase transformations were monitored throughout the experiment by x-ray absorption temperature scans [22] and x-ray diffraction measurements, collected with an area detector. Temperature scans were performed while monitoring the x-ray absorption at the energy $E^* = 8.338$ keV on the rising part of the Ni K edge chosen to maximize the absorption contrast between solid and liquid Ni. A typical temperature scan is shown in Fig. 1, left panel. The hysteresis cycle through the solid-liquid phase transition is a proof of the deep undercooling of ≈350 K

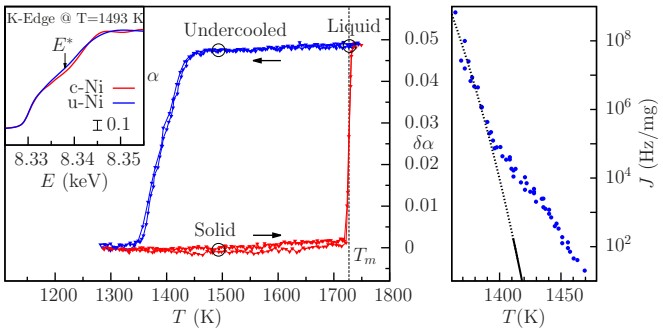

FIG. 1. (Color online) Left panel: X-ray absorption temperature scans of the Ni sample. The change of the absorption coefficient $\delta\alpha$ at $E^* = 8.338$ keV (see XAS spectra in the inset) is plotted with respect to the c-Ni absorption level during repeated thermal cycles (see arrows). The hysteresis highlights an exceptional undercooling (≈350 K) of the Ni droplets. Right panel: temperature dependence of the Ni nucleation rate from the cooling scan compared with the fitting model introduced in Ref. [5] within (solid curve) and outside (dashed curve) the previously accessed undercooling range.

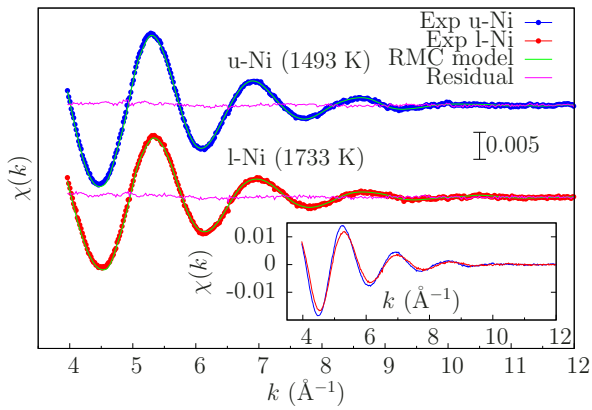

FIG. 2. (Color online) Comparison of calculated (RMC simulation, green [gray]) and experimental EXAFS $\chi(k)$ signals for u-Ni (dots, red [gray]) and l-Ni (dots, blue [gray]) at 1493 K and 1733 K respectively. The flat residual confirms the quality of the refinement. The two experimental EXAFS signals are compared in the inset.

achievable by the submicrometric Ni droplets. The molten nature of the high x-ray absorption state at E^* was also confirmed by the absence of Debye-Scherrer rings in the diffraction pattern. The sharp absorption rise at $T \simeq T_m$ is clearly associated with the melting of the fcc Ni crystal. The relatively broader decrease in absorption in the cooling process when $T \lesssim 1470$ K is associated with the progressive nucleation of the broad mass droplet distribution in the sample. Analysis of this part of the scan using previous methods [23] allows us to extract the Ni nucleation rate in a relatively wide T range. Comparison of this data with results of a previous investigation [5] (Fig. 1, right panel) indicates that the process is initially dominated by heterogeneous nucleation effects, while the tail for $T \lesssim 1400$ K is compatible with the (possibly homogeneous) nucleation rate previously observed.

XAS measurements have been collected at different temperatures: in the solid phase (c-Ni) at room temperature (300 K) and at 1493 K; in the stable liquid phase (l-Ni) at 1733 K, near the melting temperature, and in the undercooled state (u-Ni) at 1493 K.

As anticipated, RMC modeling was applied to the measured XAS data [21], using a 1372-atom cubic cell with periodic boundary conditions and fixed density. Due to the short-range nature of the XAS signal, the RMC refinement was carried out using a measured pair distribution function $g(r)$ (see Ref. [24]) only as a constraint for long-range order. A total of 100 different box configurations, obtained after convergence to a minimum and reproducing our experimental data, were finally considered.

In Fig. 2 the experimental EXAFS (extended x-ray absorption fine structure) signals of l-Ni (1733 K) and u-Ni (1493 K) are compared with the model signal for the RMC equilibrated structures. The short-range pair distribution is fully included in the simulation [13] through the irreducible two-body XAS $\gamma^{(2)}$ signals, while the three-body contribution is accounted for by a three-body Gaussian distribution of equilateral configurations, which represents the most prominent higher-order XAS signal $\gamma^{(3)}$. The results reported in Fig. 2 show that RMC simulations are able to reproduce the experimental XAS signal including the contribution of both short-range two-body and three-body distributions. The EXAFS signals of l-Ni and u-Ni show slightly different amplitude and phases highlighted in the inset of Fig. 2.

The normalized bond-angle distributions $f(\theta)$ obtained by RMC simulations of l-Ni and u-Ni, reported in Fig. 3, are those typical of a close-packed liquid metal, showing structures that were already observed in liquid and undercooled Cu [13]. The short-range pair distribution functions of l-Ni and u-Ni measured by EXAFS and reconstructed by RMC are reported in the inset of Fig. 3 and compared with previous determinations [19] of the $g(r)$ in this high-temperature liquid.

The validity of the structural results obtained by RMC data analysis have been put to a test performing molecular dynamics (MD) simulations of l-Ni and u-Ni using an empirical interatomic potential, as implemented in the LAMMPS code [25]. The interatomic potential uses a many-body potential scheme

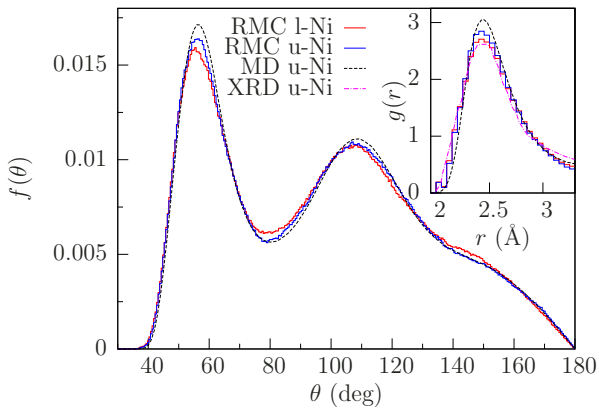

FIG. 3. (Color online) Normalized bond angle distributions $f(\theta)$ calculated from MD (dashed) and RMC configurations for u-Ni (blue [gray]) and l-Ni (red [gray]). Inset: first peak of the pair distribution function $g(r)$ obtained by RMC-XAS for l-Ni (red [gray]) and u-Ni (blue [gray]), compared with MD results (dashed) and previous XRD data [19] (dot-dashed).

to catch the essential band character of the metallic bond [26]. The equations of motion used are those of Shinoda *et al*. in Ref. [27], which combine the hydrostatic equations of Martyna *et al*. [28] with the strain energy proposed by Parrinello and Rahman in Ref. [29]. The time integration schemes closely follow the time-reversible measure-preserving Verlet and reversible reference system propagator algorithm integrators [30].

The NPT MD simulations consist in an atomic system of 4000 atoms, initially arranged randomly in a cubic cell at the experimental liquid density. Constant-temperature and constant-pressure MD simulations were performed to melt the system at high temperature ($T = 2000$ K and room pressure). During the high-temperature simulation, atoms covered a distance as long as about 50 Å, ensuring the final configuration retains no memory of the initial geometry. Then instantaneous quench was performed from the equilibrated high-temperature configuration to two temperatures: 1733 K (l-Ni) and 1523 K (u-Ni).

After 200 ps of annealing at the final temperature, statistical averages and relevant data for structural analysis have been calculated over time trajectories of 50 ps.

Bond-angle distributions of liquid Ni (within first-neighbor atoms) obtained by RMC and MD simulations are compared in Fig. 3. As a cutoff to consider first neighbors we chose the first minimum in the radial distribution function, $R_{cut} = 3.30$ Å, whose first peak is also reported in Fig. 3 (inset). The bond-angle distribution $f(\theta)$ shows a prominent peak at about 60° and a broad peak at 110°. The height of these two peaks is an indication [13] of preferential local icosahedral ordering respect to fcc-like ordering characteristic of the solid phase. The bond-angle distribution (RMC data shown in Fig. 3) displays smoother peaks in l-Ni than in u-Ni.

MD and RMC results are found to be in very good agreement both for what concerns the general shape of the pair and bond-angle distributions and for the observed trend decreasing the temperature from liquid to undercooled Ni.

Two different approaches have been used to analyze the local geometry: the common-neighbor analysis (CNA) as introduced in Refs. [31,32] and the calculation of spherical harmonics invariants as introduced in Ref. [33]. In the first analysis each pair of nearest-neighbor atoms is classified by using a set of three indexes jkl: j is the number of nearest neighbors common to both atoms, k is the number of bonds between the common neighbors, and l is the number of bonds in the longest continuous chain formed by the k bonds between common neighbors. This method is able to distinguish between various local structures: 555 pairs are characteristic of icosahedral structures (ICOS), 544 and 433 are characteristic of strongly distorted or defective icosahedra (DICOS), 666 are found in bcc structures, and 421 and 422 are characteristic of fcc and hcp ordering [19]. These geometrical structures are the most abundant in our models for liquid and undercooled Ni, and their relative weights are reported in Fig. 4, normalized to the total number of nearest-neighbor pairs.

It is evident that the highly distorted or defective icosahedra (DICOS) are the most frequent configurations (around 40%) and their presence slightly increases (by 2%) in the undercooled liquid state. Similarly nearly icosahedral structures (ICOS) increase from 11–12% in the liquid to 14–15% in undercooled Ni, indicating that ISRO is enhanced in the supercooled state. Structures representative of crystalline-like order are also found, mainly corresponding to fcc and hcp local ordering.

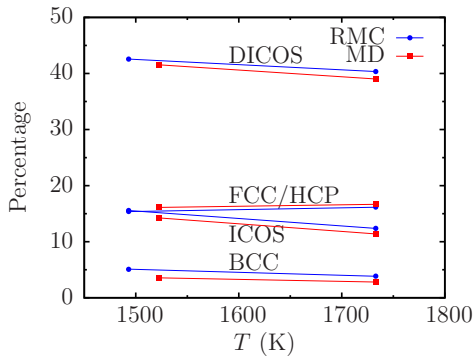

FIG. 4. (Color online) Percentage of nearest-neighbors pairs with given symmetry (CNA analysis of MD and RMC configurations). ICOS, icosahedral (555 pairs); DICOS, distorted icosahedral (544 and 433 pairs); BCC, bcc (666 pairs); and FCC/HCP, fcc and hcp (421 and 422 pairs).

The structural models have been also analyzed by another method, used previously for liquid and undercooled Cu [13–15]. Within this method, a set of bond order parameters is calculated for each atom, depending on the orientation of the vector joining the atom with its nearest neighbors within the cutoff. In particular we considered the $\hat{W}_6$ parameter for its high sensitivity to icosahedral symmetry ($\hat{W}_6 = -0.169754$ for a perfect icosahedron, $\hat{W}_6 \sim 0$ for other structures [33]). The normalized $\hat{W}_6$ parameter distributions for u-Ni are shown in Fig. 5. The MD and RMC distributions are slightly different but have the same shape and behavior, extending towards the icosahedral value. As shown in Ref. [13], a reasonable upper limit to consider icosahedral and nearly icosahedral configurations is $\hat{W}_6 = -0.09$. Using this criterion, the ISRO fraction is around 14% in the RMC configurations and around 18% in the MD configurations for undercooled liquid u-Ni. Practically no differences were found for the stable liquid (l-Ni) in both cases. Clearly, those results are compatible with

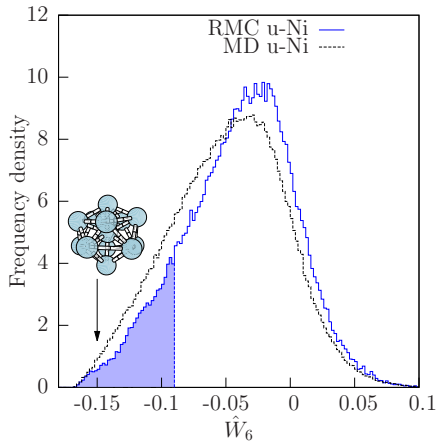

FIG. 5. (Color online) Normalized distribution of the spherical invariant $\hat{W}_6$ calculated from MD and RMC configurations in u-Ni.

the number of ICOS structures found by the CNA analysis shown in Fig. 4, showing that the two methods are both useful tools for detecting nearly icosahedral configurations. Highly distorted or defective icosahedral configurations (DICOS) detected by CNA analysis are merged in the $\hat{W}_6$ distribution that shows more stringent conditions for the identification of icosahedral symmetry.

In conclusion, we have evaluated the presence and amount of ISRO in liquid and undercooled Ni by combining the XAS, RMC, and MD techniques. Different indicators for local geometry (spherical invariants and CNA) have been used which give consistent results for both liquid and undercooled liquid Ni. The fractions of fivefold nearly icosahedral configurations were in the ranges 14–18% for u-Ni and 11–14% for l-Ni respectively. The emerging picture for the liquid structure is that of a mixture of nearly icosahedral structures embedded in a disordered network mainly composed of fragments of highly distorted icosahedra (indicated by 544 and 433 pairs, 40–45% of the total), structures reminiscent of the crystalline phase (422 and 421 pairs), and other configurations.

[1] F. C. Frank, Proc. R. Soc. London A **215**, 43 (1952).
[2] D. Turnbull and R. E. Cech, J. Appl. Phys. **21**, 804 (1950).
[3] K. F. Kelton and A. L. Greer, *Nucleation in Condensed Matter* (Elsevier, Amsterdam, 2010).
[4] A. Filipponi, A. Di Cicco, and E. Principi, Phys. Rev. E **86**, 066701 (2012).
[5] J. Bokeloh, R. E. Rozas, J. Horbach, and G. Wilde, Phys. Rev. Lett. **107**, 145701 (2011).
[6] P. J. Steinhardt, D. R. Nelson, and M. Ronchetti, Phys. Rev. Lett. **47**, 1297 (1981).
[7] S. Nosé and F. Yonezawa, J. Chem. Phys. **84**, 1803 (1986).
[8] H. Jónsson and H. C. Andersen, Phys. Rev. Lett. **60**, 2295 (1988).
[9] T. Kondo and K. Tsumuraya, J. Chem. Phys. **94**, 8220 (1991).
[10] S. Mossa and G. Tarjus, J. Chem. Phys. **119**, 8069 (2003).
[11] A. Filipponi, J. Phys.: Condens. Matter **13**, R23 (2001).
[12] A. Filipponi, A. Di Cicco, and S. De Panfilis, Phys. Rev. Lett. **83**, 560 (1999).
[13] A. Di Cicco, A. Trapananti, S. Faggioni, and A. Filipponi, Phys. Rev. Lett. **91**, 135505 (2003).
[14] P. Ganesh and M. Widom, Phys. Rev. B **74**, 134205 (2006).
[15] M. Celino, V. Rosato, A. Di Cicco, A. Trapananti, and C. Massobrio, Phys. Rev. B **75**, 174210 (2007).
[16] N. Jakse and A. Pasturel, J. Chem. Phys. **120**, 6124 (2004).
[17] N. Jakse and A. Pasturel, J. Chem. Phys. **123**, 244512 (2005).
[18] T. Schenk, D. Holland-Moritz, V. Simonet, R. Bellissent, and D. M. Herlach, Phy. Rev. Lett. **89**, 075507 (2002).
[19] T. Kim and K. Kelton, J. Chem. Phys. **126**, 054513 (2007).
[20] R. L. McGreevy and L. Pusztai, Molec. Simul. **1**, 359 (1988).
[21] A. Di Cicco and A. Trapananti, J. Phys.: Condens. Matter **17**, S135 (2005).
[22] A. Filipponi *et al.*, Rev. Sci. Instrum. **71**, 2422 (2000).
[23] S. De Panfilis and A. Filipponi, J. Appl. Phys. **88**, 562 (2000).
[24] Y. Waseda, *The Structure of Non-crystalline Materials* (McGraw-Hill, New York, 1980).
[25] S. Plimpton, J. Comp. Phys. **117**, 1 (1995).
[26] S. M. Foiles, M. I. Baskes, and M. S. Daw, Phys. Rev. B **33**, 7983 (1986).
[27] W. Shinoda, M. Shiga, and M. Mikami, Phys. Rev. B **69**, 134103 (2004).
[28] G. J. Martyna, D. J. Tobias, and M. L. Klein, J. Chem. Phys. **101**, 4177 (1994).
[29] M. Parrinello and A. Rahman, J. Appl. Phys. **52**, 7182 (1981).
[30] M. E. Tuckerman *et al.*, J. Phys. A: Math. Gen. **39**, 5629 (2006).
[31] J. D. Honeycutt and H. C. Andersen, J. Phys. Chem. **91**, 4950 (1987).
[32] A. S. Clarke and H. Jonsson, Phys. Rev. E **47**, 3975 (1993).
[33] P. J. Steinhardt, D. R. Nelson, and M. Ronchetti, Phys. Rev. B **28**, 784 (1983).